Conformation Dependence of Electronic Structures of Poly(ethylene oxide)

B. Brena,[†] G. V. Zhuang,[‡] A. Augustsson,[§,⊥] G. Liu,[||] J. Nordgren,[⊥] J.-H Guo,[§] P. N. Ross,[‡] and Y. Luo*,[†]

Theoretical Chemistry, Royal Institute of Technology, SE-10691, Stockholm, Sweden, Materials Sciences Division, Lawrence Berkeley National Laboratory, Berkeley, California 94720, Advanced Light Source, Lawrence Berkeley National Laboratory, Berkeley, California 94720, Department of Physics, Uppsala University, P.O. Box 530, SE-75121, Uppsala, Sweden, and Environmental Energy Technologies Division, Lawrence Berkeley National Laboratory, Berkeley, California 94720

Received: September 22, 2004; In Final Form: February 25, 2005

The electronic structure of pure poly(ethylene oxide) (PEO) for four different polymeric chain conformations has been studied by Hartree−Fock (HF) and density functional theory (DFT) through the analysis of their valence band photoelectron spectroscopy (VB-PES), X-ray emission spectroscopy (XES), and resonant inelastic X-ray scattering (RIXS). It is shown that the valence band of PEO presents specific conformation dependence, which can be used as a fingerprint of the polymeric structures. The calculated spectra have been compared with experimental results for PEO powder.

I. Introduction

Poly(ethylene oxide) (PEO), a polymer composed by a sequence of (CH_2CH_2O) monomeric units, has many important technological applications, ranging from biocompatible materials[1] to ion conducting polymer electrolytes.[2−5] Owing to the character of dissolved alkali salts, several kinds of ion conducting polymer electrolytes can be prepared with PEO, and then employed in high energy density Li batteries and fuel cells. The structure of the polymer alkali salts complexes and its correlation with the ionic transport properties of the PEO based electrolytes have attracted considerable attention. During the past decades, experimental and theoretical works have been extensively dedicated to the geometry and the crystal growth of the pure PEO,[6−13] and the PEO conformations in polymer electrolytes.[2,14−23] Equally important in this contest is the study of the electronic structure of PEO, which would lead, for example, to a fundamental understanding of the ionic conductivity, by revealing the interactions between polymer and salt at the molecular level. The valence band of the polymer has been studied by valence band photoelectron spectroscopy (VB-PES) and X-ray emission spectroscopy (XES). Due to the sensitivity of these techniques to the geometrical structure of polymers, they can be used as a means to distinguish among different possible conformations.[24,25] In this work we have studied by theoretical means the dependence of the valence band electronic structure of PEO on the geometry of the polymeric chain upon four different conformations. We have compared our results with the experimental VB-PES presented in the literature.[24] XES allows us to investigate the element specific valence band structure and it has previously shown its sensitivity to different molecular structures.[26] Moreover, the resonant X-ray emission, also known as the resonant inelastic X-ray scattering (RIXS), is particularly sensitive to the molecular symmetry. We have simulated XES and RIXS spectra for all the models considered, and compared them with the experimental results from a PEO powder sample. By applying these techniques, we have observed that morphological changes in the polymer can affect the valence band structure. In other words, the change of electronic structures can thus be used as a fingerprint to identify the structural conformation of the polymer, and in turn to gain insights on the interplay between morphology and electronic structure.

II. Structures of the Pure PEO

The structural models under investigation are displayed in Figure 1. We have considered four different conformations of the PEO polymer, of the types proposed in the past based on X-ray diffraction, Raman, and infrared spectroscopy (IR) studies.[6,8] Two of them are related to the pure PEO, and the other two have been proposed for PEO in several complexes. Being the polymer chain composed of a sequence of (CH_2CH_2O) units, the conformations about the successive OCCO, CCOC, and COCC segments are defined to be trans (T) if the dihedral angle between the four atoms is zero, and consequently the four atoms are coplanar, and to be gauche (G), if the dihedral angle differs from zero. According to the rotation direction, the gauche can be labeled G^+ (or simply G) or G^-. The structural models in Figure 1 are characterized by different sequences of T and G^+ or G^- elements that lead to very different polymeric structures. The pure PEO crystal is known to have the structure of a helix, as determined by Takahashi and Tadokoro in 1973 by X-ray diffraction analysis.[7] The monomeric units are repeated seven times in two complete turns of the helix. The PEO helix is slightly distorted with respect to a D_7 point group, and the monomeric units are repeated in T_2G sequences.[7] We will refer to this model as the *helix*. The PEO chains have shown also another type of arrangement, in the form of a planar zigzag chain, where all the monomeric units are aligned in the trans

[†] AlbaNova University Center.
[‡] Materials Sciences Division, Lawrence Berkeley National Laboratory.
[§] Advanced Light Source, Lawrence Berkeley National Laboratory.
[⊥] Uppsala University.
[||] Environmental Energy Technologies Division, Lawrence Berkeley National Laboratory.

10.1021/jp045685u CCC: $30.25
Published on Web 04/02/2005

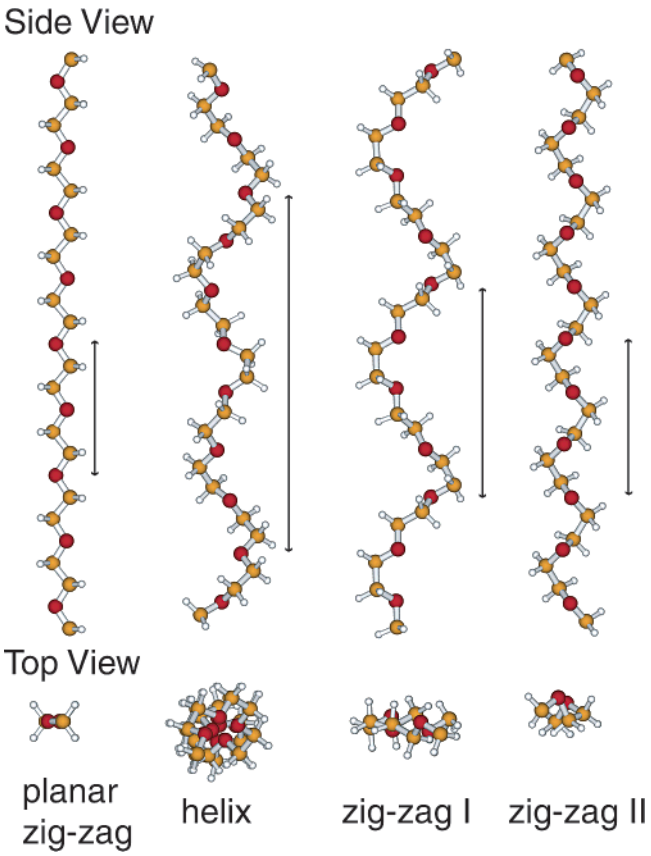

Figure 1. Side and top view of the structures of the four model systems. On the side of the polymeric chains, a line indicates the dimension of the repeating units of each conformation along the chain length direction.

configuration, resulting in a chain of coplanar oxygen and carbon atoms (*planar zigzag* model). This planar zigzag geometry has been observed in a stretched sample fixed on a sample holder under tension, where it was converting to the helix structure when the tension was released.[6] Moreover, PEO has been observed to adopt a planar zigzag structure upon blending[15] and, more recently, in freeze-dried PEO, prepared in a diluted benzene solution, in which case it is a stable conformation also at room temperature.[11] Two more models were proposed, with different T and G sequences, for PEO in complexes.[6] The first one, or *zigzag I*, was proposed based on IR analysis in the PEO−$HgCl_2$ type complex,[14] and it has been proposed also as a model geometry of PEO inserted into the interlamellar space of $CdPS_3$, preintercalated with hydrated alkali cations.[21] In this structure the T and G alternate in a T_5G conformation. The second type of arrangement, or *zigzag II*, has a conformation of the kind $TG_2TG_2^-$, and has been proposed for a PEO $HgCl_2$ complex[6] and, under tension, for a PEO sodium thiocyanate (NaSCn) complex.[16] Among the four conformations described, the helix (T_2G), the zigzag I (T_5G), and the zigzag II ($TG_2TG_2^-$) are formed by different conformations of T and G monomeric units, while the planar zigzag is only formed by T monomeric units. As illustrated in Figure 1, zigzag I and zigzag II could be described as compressed helix compared to the more open helix configuration found in PEO crystal. All the models have been included in our study, to test the sensitivity of the X-ray spectroscopies to chain structures of alternating T and G monomers in different fashions and with different relative abundance. In the calculations we have assumed that these structures are randomly oriented in space.

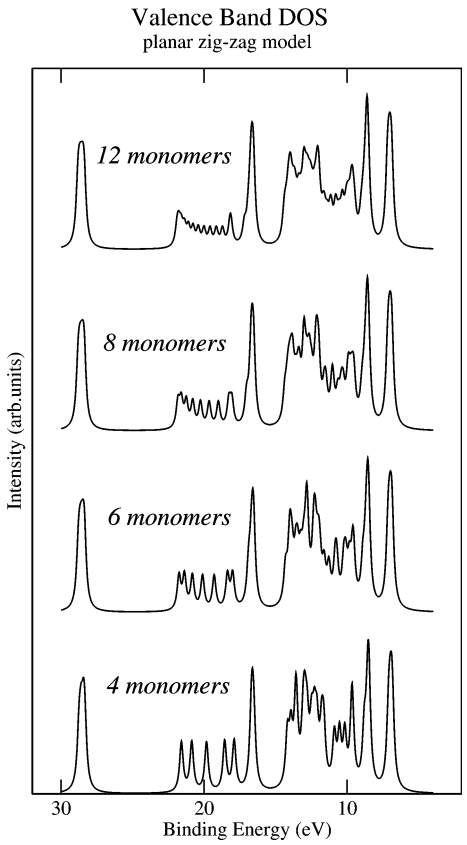

Figure 2. Length dependence of the VB-DOS. Oligomers with 4, 6, 8, and 12 monomers are calculated.

III. Theoretical Methods

In this work we have simulated the polymer VB-PES, XES, and RIXS, by using three different codes at different theory levels. Oligomers formed by 12 monomer units and terminated by the methyl group (CH_3) at both ends have been chosen for all spectral calculations, which is consistent with, yet more stringent than another previous work.[27] The size of the oligomers has been chosen by examining the length dependence of the valence band density of states (DOS) of planar zigzag chains. The DOS of oligomers of size varying from 4 to 12 monomer units have been calculated by using the hybrid density functional theory (DFT) at the B3LYP level with the 6-31G basis set as implemented in the GAUSSIAN98 code,[28] and have been compared to each other. The computed lines have been convoluted by a Lorentian curve of 0.15 eV full width at half-maximum (fwhm), simulating the lifetime broadening. The results, illustrated in Figure 2, show that the evolution of the spectral features is completed at about 8 monomer units as the DOS of them is almost identical with that of the 12 monomer units. The valence band molecular orbitals have been computed on the basis of the Koopman's theorem at the B3LYP/6-31G level, using the GAUSSIAN98 code. We have adopted the Gelius model[29] to simulate the valence band XPS spectra. The theoretical photoionization cross sections for each atomic orbital[30] and a Lorentzian profile of 0.15 eV fwhm have been used to generate the spectra. The calculated spectra are compared with previous experimental results obtained at the Al Kα excitation energy.[24] When comparing the theoretical results with experimental spectra, there are often differences in the energy scales of the order of a few electronvolts, due to the fact that the Koopman's approximation does not apply exactly to the Kohn−Sham orbitals, and that our computational model does not account for the relaxation effects. In this comparison we

have therefore aligned the theoretical energies to the experimental ones, by applying a rigid shift of 2 eV. The calculations of the nonresonant and resonant XES and RIXS have been performed by the Dalton code[31] at the Hartree−Fock (HF) theory level with the group theory formulation developed by Luo et al.[32,33] HF is the only theory available for RIXS calculations of such large systems at the moment. The ground-state electronic structure is used to compute the intensities (adiabatic approximation). The 6-31G bases set has been employed in the computations of the transition moments and of the orbital energies. In the nonresonant regime, we calculate the transition moment between valence and core orbitals, while in the resonant regime we moreover account for the interference between scattering channels. The RIXS spectra are calculated for the case of resonant excitation to the lowest unoccupied molecular orbital (LUMO). As in the case of the VB-PES calculations, the computed spectra have been convoluted by a Lorentzian profile with a fwhm of 0.15 eV. The calculated carbon and oxygen X-ray emission spectra included all the symmetry inequivalent carbon and oxygen atoms in PEO for all four structural models. The valence band obtained at the HF level for large systems such as polymers is known to be too broad due to the lack of electron correlations, and therefore it is common practice to contract the calculated curves by a factor between 1.15 and 1.3, to reproduce the energy dispersion of the experimental spectra.[33−35] In our case, the best agreement is obtained for a contraction factor of 1.3. We have also studied the valence band structure in a polymer of infinite length, using the periodic DFT code Dacapo.[36] The energy resolved p density of states (pDOS) projected onto the atomic orbitals are used to represent the nonresonant XES spectrum. In the periodic approach, a unit cell is replicated along with the three spatial dimensions to build an infinite periodic structure: in this case, the unit cell is formed by the repeating sequence of the polymer models, to form infinite long polymer chains with an interchain distance of about 5 to 6 Å. This distance is determined by the van der Waals radius of the outermost elements, which is also consistent with the crystal structure of PEO in helical form.[7] The repeating unit cell is different for different models: a seven-monomer unit cell is used for the helix, a four-monomer unit is used for the zigzag I model, and two-monomer units are used for the planar zigzag and for the zigzag type II (see Figure 1). The Dacapo code uses a plane wave approach to describe the valence electronic states and Vanderbilt ultrasoft pseudopotentials for the core−electron interactions.[37] In the calculations we have used a cutoff energy of 340 eV, and the Monkhorst Pack k-points sampling.[38]

IV. Experimental Section

Commercial poly(ethylene oxide) (PEO) powder with average molecular weight of ca. 600 000 (Aldrich) was purified to remove the inhibitor. The purified PEO powder was thoroughly dried and stored in a glovebox. The infrared spectra obtained from the PEO powder prepared as described above indicate that the powder is free of water and solvents. Differential scanning calorimetry (DSC) measurement was performed with a Perkin-Elmer DSC7 Calorimeter. The PEO powder (3.6 mg) was sealed in an aluminum pan inside a He filled glovebox. The measurement was carried out under nitrogen flow at a 10 °C/min heating rate in the interval −150 to 100 °C. The PEO powder exhibits a pronounced endothermic peak at 66.5 °C, due to its well-known crystalline-amorphous transition, with heat of fusion of 107.8 J/g. Based on the reported theoretical heat of fusion of 203 J/g[39,40] for 100% crystallized PEO, the PEO powder used in this work was determined to contain approximately 53% of the crystalline phase. The dry PEO powder was mounted onto Indium foil in a glovebox and then transferred to the ultrahigh vacuum (UHV) chamber under a base pressure of 10^{-9} Torr. Similar procedures have also been applied to a crystallized PEO thin film. The XES and RIXS were obtained at beamline 7.0[41] of the Advanced Light Source (ALS), Lawrence Berkeley National Laboratory. Emission spectra were acquired with a high efficiency grazing incidence X-ray spectrometer.[42] The combined monochromator and spectrometer energy resolution was estimated to be 0.4 and 0.7 eV for carbon and oxygen, respectively. The nonresonant carbon K-edge emission (carbon XES) was measured with photon excitation energy of 320.0 eV while the resonant carbon K-edge emission (carbon RIXS) was measured with excitation energy of 281.0 eV. The oxygen K-edge XES and RIXS spectra were excited with photon energies of 573.3 and 532.0 eV, respectively.

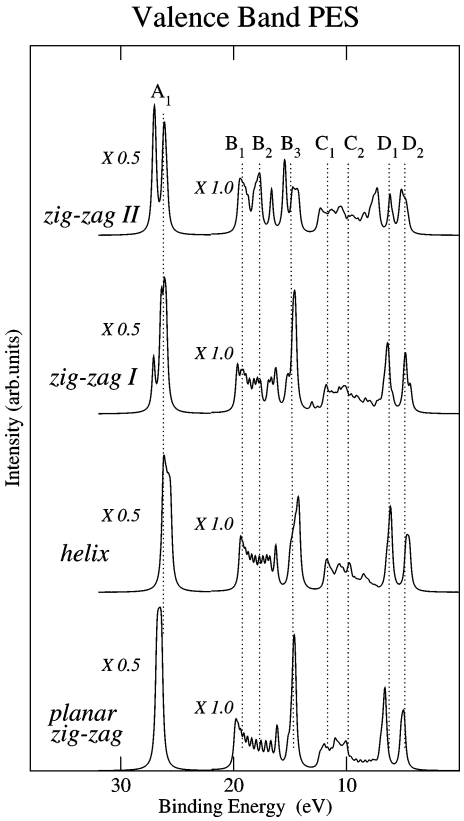

Figure 3. Calculated VB-PES for the four models. A_1 to D_2 are the most prominent peaks which correspond to the ones in ref 24.

V. Results and Discussion

A. Valence Band Photoelectron Spectroscopy. The calculated VB-PES for the four models of the PEO are illustrated in Figure 3. The most prominent features of the spectra are noted in the figure as the A to D peak groups, and, as can be seen in Table 1, they compare well with those observed in previous VB-PES of PEO film in the work of Boulanger et al.,[24] who performed Hartree−Fock calculations of the VB-PES spectra with the STO-3G basis set for a planar zigzag model of PEO and compared them with the experiment. Their results for the planar zigzag are in very good agreement with those of the present study. We have moreover performed the VB-PES calculations for the other three structures discussed above. It is evident from Figure 3 that there are some remarkable differences among the spectra of the four PEO models, although the main

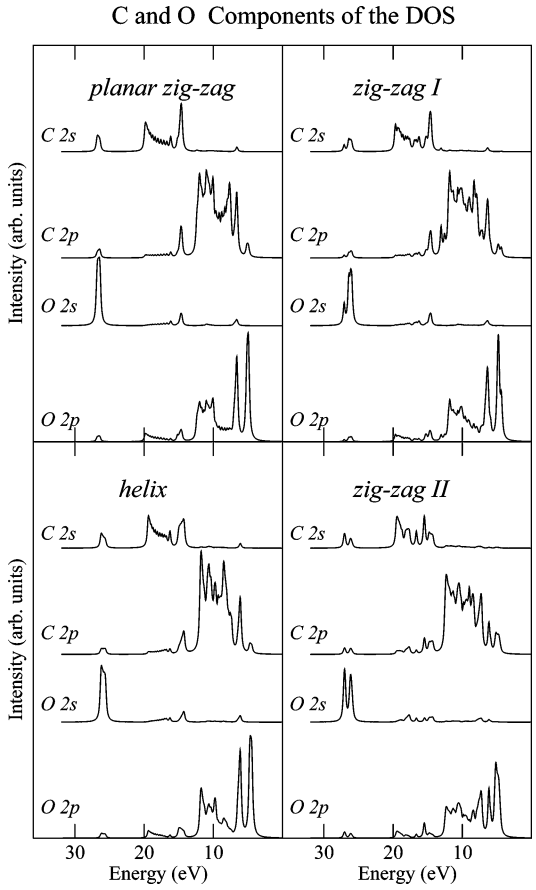

Figure 4. The carbon and oxygen 2s and 2p composition of the DOS in four models.

TABLE 1: The Experimental and Theoretical Binding Energies (in eV) of the Main Spectral Features in the VB-PES of PEO

peak label	experiment[a]	planar zigzag	helix	zigzag I	zigzag II
D_2	4.49	4.5	4.5	4.5	4.5
D_1	6.35	6.2	6.1	6.2	5.7/7.3
C_2	9.49	10.0	9.7	10.1	10.1
C_1	11.35	11.3	11.5	11.4	11.5
B_3	14.57	14.2	14.4	14.5	14.0/14.8
B_2	17.51	18.0	17.8	17.8	17.4
B_1	18.58	19.0	19.1	18.9	18.6
A_1	26.30	26.0	25.8	26.1	25.6/26.5

[a] Data taken from ref 24.

spectral lines are situated generally at similar energies, very close to the experiment (see Table 1). The spectra of the helix and the zigzag I models are very similar to each other, but they show differences with the planar zigzag and the zigzag II. In the planar zigzag there is a dip in intensity between about 7 and 9 eV, which is unique to this structure. The zigzag II spectrum is instead characterized by a larger number of peaks, and some lines, visible also in the spectra of the other models, are doubled (A_1, B_3, D_1). A detailed orbital analysis was given by Boulanger et al.[24] for the planar zigzag model. We therefore briefly discuss only the main characteristics and compare the different models.

In Figure 4 we show the population distribution of the 2s and 2p components of the oxygen and carbon in the valence band for the four models. To understand the orbital composition of each spectral profile, only the pure partial density of states is given. The analysis of the most important peaks of the spectra (A_1 to D_2), based on the spectra of Figure 3 and Figure 4, remarks the differences in the results for the four models. The

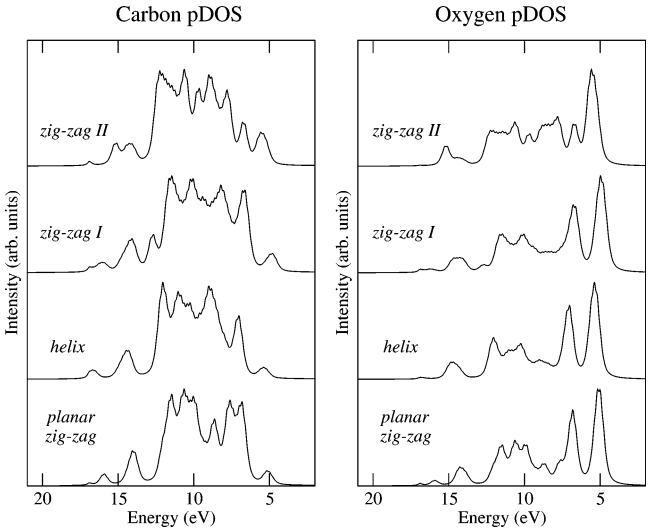

Figure 5. Carbon and oxygen pDOS for infinite polymer chains obtained from periodic DFT calculations.

peak A_1 at about 26 eV appears in all the spectra, and becomes richer in features by going from the planar zigzag to the zigzag II. This peak is mainly formed by the oxygen 2s orbitals with a very small contribution of carbon 2s (see Figure 4). The structures in the energy region 13−20 eV (peaks B) are also very different in the zigzag II model (five peaks) with respect to the other models. The peak B_2 is distinguishable only in the zigzag I and II, and it is smeared out with a number of other equally intense structures in the helix and in the planar zigzag. This energy region is mostly characterized by σ CO, CC, and CH bond. The peak B_2 has a much smaller intensity in the spectrum of the planar zigzag model; the same observation was reported in ref 24. It is noticeable in Figure 3 that the intensity of the peak B_2 is higher in the helicoidal type models. The peaks denoted as C_1 and C_2 are visible in all the structures, but actually, according to the calculations, this energy region is populated by three small peaks rather than two. In this energy interval most of the CO and CC bonds are formed by the 2p of oxygen and carbon atoms. At about 7 to 9 eV, between the peaks C and D the planar zigzag spectrum shows a large dip in intensity, unlike the other models. This region is populated by CC, CO, and CH bonds with 2p character. The last two peaks D_2 and D_1 are similar for all the structures but the zigzag II, where D_1 peak splits into two components. The D_1 peak is formed by O 2p and C 2p, while the D_2 is formed mostly by O 2p, and is identified as the oxygen lone pair.

The effects of intermolecular interaction in the condensed phase have been analyzed by studying the carbon and oxygen pDOS calculated for periodic polymeric chains by Dacapo, shown in Figure 5. The pDOS of carbon and oxygen calculated with Dacapo are analogous to the pDOS represented in Figure 4 calculated with the GAUSSIAN98 code for 12 monomer units of PEO oligomers, confirming that the 12 monomer models are adequate to represent a polymer sample in the condensed phase. Both these calculations are performed at the DFT theory level. It can be concluded from our analysis that there are some features that differentiate significantly the valence band structure of the various models, in dependence of the geometrical arrangement of the polymeric chain. It is possible to distinguish between a planar zigzag and a helicoidal type conformation, and, among the helicoidal ones, the zigzag II possesses unique features. The orbitals that have a large spatial component perpendicular to the length of the polymer, like the CH or the oxygen lone pair, can be more affected by a closer turning of

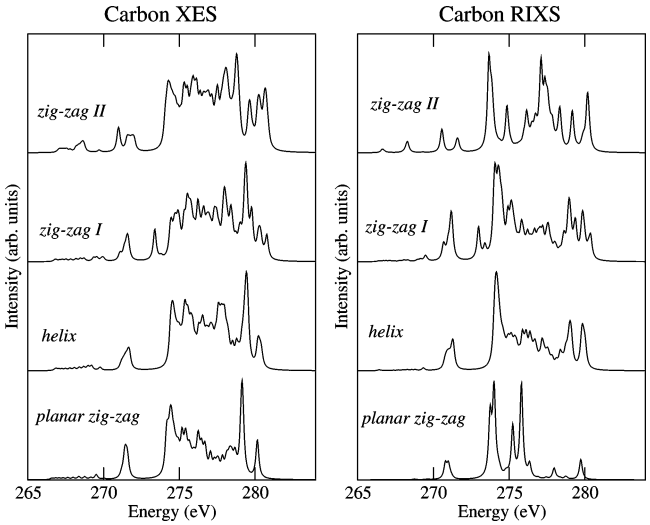

Figure 6. Calculated carbon XES and RIXS spectra of the four models.

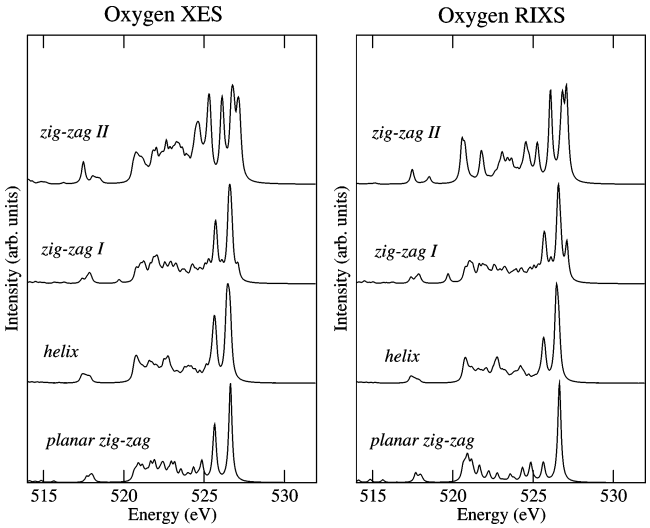

Figure 7. Calculated oxygen XES and RIXS spectra of the four models.

the molecule, where they may come close to other segments of the chain, and subject to more interactions.

B. X-ray Emission Spectra. The X-ray emission spectroscopy is an element selective technique that probes the partial density of states of p character at a particular atomic center in the valence band, as a result of the radiative decay of a valence electron into a core hole. With this technique we can thus separately obtain the X-ray emission spectra of the carbon and oxygen atoms of the polymeric chains. We have computed the nonresonantly and resonantly excited X-ray emission spectra of carbon and oxygen for the four conformations described above, and the results of our calculations are shown in Figures 6 and 7. The X-ray emission spectra compare well with the Dacapo calculated pDOS reported in Figures 4 and 5: although the XES should be represented by the transition moment between core and valence orbitals, the pDOS can be considered as the first-order approximation. The discrepancies between the two different descriptions are attributed both to the difference in the HF and DFT methods used, and to the fact that the transition moment is sensitive to the local molecular symmetry.

1. Carbon Spectra. In Figure 6 are shown the theoretical XES and RIXS spectra of carbon calculated for the 12 unit oligomers for all the structures. The nature of the peaks in the XES spectra is analogous to the one reported for the VB-PES, but in this case only the 2p orbitals are present. The XES and RIXS calculations show some remarkable differences for the four models. By analyzing the spectra of all the models, one can notice that the presence of rather high intensity features at about 278 eV is a characteristic of the helicoidal type structures. In this energy region, populated mostly by CO, CC, and CH bonds, the planar zigzag shows, instead, a considerable decrease in intensity. The same characteristic were observed also in the VB-PES in the region between 7 and 9 eV of Figure 3 and 4, and it is present in the pDOS of the planar zigzag model in Figure 5. The RIXS implies stricter symmetry selection rules, and consequently a lower number of features are present in the spectra. In the carbon RIXS (in Figure 6) the depression of the intensity of many peaks of the nonresonant case is evident, especially for the planar zigzag conformation, which has the highest degree of symmetry of all the models considered. Also in this case, as for the XES, some characteristics of the spectra differentiate the planar zigzag model from the others. In the helix and in the zigzag I and II, the peaks at higher energy (e.g. in the spectral region between about 278.5 and 281 eV) are more intense than those in the planar zigzag. Furthermore, the spectrum of the planar zigzag is characterized by two almost equal intensity peaks centered at about 273.9 and 275.8 eV and the features at higher energies have drastically reduced their intensity in comparison with all the other structures. A second high-intensity peak is visible also in the spectrum of the zigzag II, at about 277.2 eV. The considerable differences that one can observe between the resonantly and nonresonantly excited emission spectra of carbon indicate that these are very sensitive to the local symmetry of the carbon atoms.

2. Oxygen Spectra. The calculated results for the X-ray emission of oxygen are illustrated in Figure 7. In all nonresonant spectra, one can see a high-intensity feature at about 526.5 eV, corresponding to the oxygen lone pair. Except for the zigzag II model the second peak at 525.5 eV is less intense, and in all the spectra many smaller peaks of similar intensity are present in the energy region extending down to about 520 eV. The XES of the zigzag II conformation shows several distinctive spectral features between 525 and 527.5 eV, in addition to the higher intensity weight below 524 eV with respect to oxygen lone pair.

The calculated RIXS for all the models considered (Figure 7) show better defined spectral features compared to XES. As for the carbon, and as a result of the stricter selection rules of the RIXS process, several spectral features found in the XES disappear in the RIXS spectra. Furthermore, the difference among the four conformations is evident in the calculated RIXS. Specifically, as for the oxygen XES, the lone pair orbitals of the oxygen atoms are very sensitive to the presence, in their vicinity, of other atoms of the chain, as reflected by the changes in the spectral distribution of the different models in the energy region between 526 and 528 eV. Although the helix and the zigzag I show only subtle discrepancies in the spectral region below 525 eV, a unique feature at 527.1 eV in the zigzag I allows us to differentiate the two conformations by taking advantage of the symmetry selectivity of RIXS.

3. Comparison with the Experiment. As a first of such studies, we have used the theoretical XES and RIXS to characterize the conformation of a PEO powder sample. So far, to simulate the spectra corresponding to the PEO samples, we have used the theoretical results obtained for the four models, as building blocks for the experiment, and we have mixed them in percentages corresponding to the crystalline versus amorphous composition of the sample. Although this approach allows us

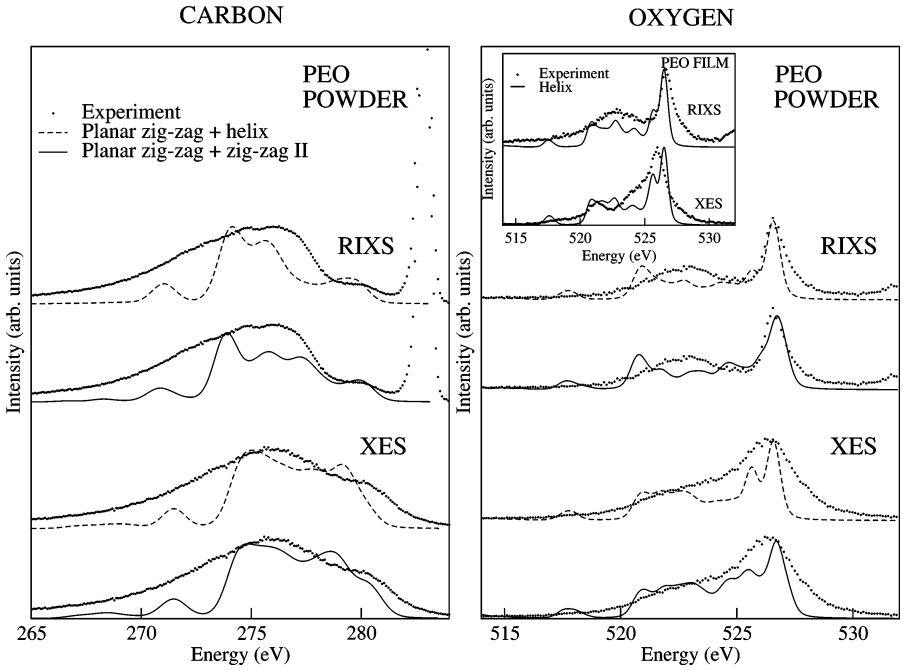

Figure 8. Comparison of the experimental results of XES and RIXS obtained for PEO powder (dotted line), with the theoretical simulations resulting by mixing in equal percentages the planar zigzag with the zigzag II (solid line) and the planar zigzag with the helix (long dashed line). At 283 eV in the carbon RIXS spectra the elastic peak is visible. In the insert are shown the experimental XES and RIXS spectra measured on a PEO film (dotted line). They are compared with theoretical curves calculated for the heliptical model (solid line).

to reproduce the most important features of the spectra, a statistical method will be employed in the future to analyze the composition of the samples, to obtain more accurate quantitative results. It is known that there exists both crystalline and amorphous phases in PEO powder, although the crystalline fraction differs depending on the molecular weight, thermal history, and level of impurities. From the DSC measurement, it is estimated that the PEO powder used in this work contains approximately 50% crystalline fraction. However, the conformation of the PEO powder is yet to be determined. In Figure 8 we present the comparison between the theoretical and experimental X-ray emission spectra for the PEO powder.

The calculated spectra of carbon XES and RIXS (Figure 6) and those of oxygen XES and RIXS (Figure 7) for each conformation were further broadened by convolution with a Gaussian curve. A fwhm of 0.7 eV was used for the oxygen, comparable to the experimental energy resolution, and a fwhm of 1.4 eV for the carbon, comparable with the much broader experimental spectra. The carbon orbitals are strongly hybridized and less localized. They are thus affected mostly by the presence of the vibronic couplings that are not considered in this work. By applying the scale factor related to the crystalline and amorphous fractions as measured from DSC, either one of the conformations helical, zigzag I, and zigzag II was chosen to represent the crystalline fraction, and the planar zigzag was chosen to represent the amorphous phase. The pure crystalline PEO has been identified as a helix formed by a succession of TTG conformers, and all the helicoidal models considered are composed of sequences of both T and G monomers. Studies analyzing the abundance of the T and G conformers in PEO samples have shown that the amount of G conformers is related to the percentage of crystalline phase in the sample with respect to the amorphous phase.[43] Consequently, a less crystalline, and more amorphous, sample is expected to present a lower amount of G and a higher amount of T conformers. In our models, the amorphous PEO powder sample used in our experiment is thus best described by the planar zigzag model.

In Figure 8 is presented the combination of 50% of zigzag II and 50% of planar zigzag, which yields the overall optimum agreement between weight-summed spectra (solid line) and experimentally measured spectra (dotted line). We compare these results, always in Figure 8, with the combination of the of 50% of helix and 50% of planar zigzag (long dashed line), as the helix is the model for the pure crystalline PEO. It is evident, especially in the XES oxygen spectra, that this second combination is worse at replicating the spectrum profile of the PEO powder, showing the important role played by the zigzag II to reproduce the XES oxygen powder experiment. Another important observation is that the experimental X-ray emission spectroscopies are indeed sensitive to the amount of crystalline phase in the PEO sample. To illustrate this point, we show oxygen XES and RIXS results for a PEO film in the insert of Figure 8. The PEO film is characterized by a high amount of crystallinity. The XES spectrum of the PEO film is very different from the powder spectrum, both in the region between 520 and 523 eV, where it has lower intensity, and around the maximum, where it is much narrower. The spectra of the PEO film are better reproduced by the calculations of the pure helix model, especially in the RIXS regime.

In the PEO powder, the validity of the conformation composed of 50% of zigzag II and 50% of planar zigzag comes from the agreement between the theory and the experimental oxygen XES in the 524 to 526 eV energy region. The combination of the planar zigzag model with either helix or zigzag I conformations would not capture the experimental intensity distribution in this region. Furthermore, the above combination conformation also presents the best agreement with the strongest peak centered at approximately 527 eV, oxygen lone pair, in experimentally measured RIXS. In light of the RIXS sensitivity toward the oxygen lone pair in polymer conformations as revealed by theoretical calculations, it appears that planar zigzag and zigzag II are the most dominant conformations in PEO powder. The experimental carbon XES and RIXS spectra measured from the PEO powder sample are

mainly composed of two broad peaks: a stronger peak at 276 eV and a less intense peak at 280 eV. The energy scale of the RIXS spectrum has been calibrated with respect to the Raman law. As the emission spectrum is collected in resonant condition, the intensity of the latter peak is greatly suppressed. Such a pronounced intensity decrease in RIXS could be attributed to the preferential excitation of planar zigzag conformation. Of all the models calculated, the carbon in the planar zigzag conformation has the highest symmetry, therefore should give rise to the strongest resonant feature in light of the symmetry sensitive nature of the RIXS. The remaining intensity of 280 eV in carbon RIXS is most likely coming from the contributions from zigzag II, consistent with the observations from oxygen RIXS and XES. Although it is not possible to exhaust all possible polymer conformations, the utilization of the model systems does reveal in unprecedented detail the conformation of PEO powder in semicrystalline form through its electronic structure. The analysis of the conformation dependent aspects of the electronic structure of the PEO models, in fact, gives us complementary information about the polymer structure. While the carbon emission spectra reflect the local symmetry around the carbon atoms, the oxygen spectra are strongly affected by the torsion of the helix, due to the localized molecular orbitals of the oxygen atoms. From comparison between the calculations and the experimental spectra of PEO powder, it appears that the spectra of the oxygen, characterized by more localized orbitals, present better agreement than carbon spectra, which are limited by neglecting of the strong vibronic couplings in the theoretical models.

Our results provide a refined description of semicrystalline PEO powder conformation, in which two conformations, i.e., helical and linear, coexist. While the amorphous phase is mostly represented by the planar zigzag conformation, the zigzag II conformation most likely, although maybe not exclusively, represents the crystalline phase in such polymer powder, instead of the helix characterized by T_2G sequences as found in the single crystal. In PEO powder the crystalline fraction of the polymer chain has more freedom to relax compared to the highly crystalline phase or under boundary conditions such as in the presence of a surface. Therefore, it seems to be reasonable to expect that the fully relaxed polymer under less restrictions would have a more closed conformation, consistent with the most closed helix among the three: zigzag II.

VI. Conclusions

The electronic structure of the PEO polymer was investigated by simulating the valence band photoelectron spectroscopy, as well as XES and RIXS spectra at the oxygen and carbon K-edge. We have modeled the PEO with four previously proposed conformations, and compared the computed spectra with the experimental results. The analysis of our results shows that the spectral features in the valence band are sensitive to the PEO conformations, thus providing a means to distinguish between planar and helicoidal structures. Such sensitivity is revealed in more detail by the atomic and symmetry selective XES and RIXS. Specifically, the analysis of the atom selective emission spectroscopy not only gives us a way to understand the molecular origin of these features, but also allows us to explore the conformation in greater detail. As a result of experiment and theory comparison, a refined description of the semicrystalline morphology emerges, in which the amorphous phase adopts a planar zigzag conformation, while the zigzag II is the dominant conformation. As such, we demonstrated the potential of X-ray emission spectra in studying the conformation of polymeric systems. More experimental and theoretical work is underway to extend this approach to study various single-phase systems such as PEO film.

Acknowledgment. This work was supported by the Carl Trygger Foundation (CTS). The authors would like to thank J. Kerr for providing the materials used in this work and for the many discussions. G.V.Z. and P.N.R. acknowledge financial support from the Chemical Sciences Division of the U.S. Department of Energy under contract No. DE-AC03-76SF00098. The Advanced Light Source (ALS) is supported by the Office of Basic energy Sciences, Materials Science Division, of the U.S. Department of Energy under Contract No. DE-AC03-76SF00098.

References and Notes

(1) Gong, X.; Dai, L.; Griesser, H. J.; Mau, A. W. H. *J. Polym. Sci., Part B*: *Polym. Phys.* **2000**, *38*, 2323.
(2) Johnson, J. A.; Saboungi, M.-L.; Price, D. L.; Ansell, S. *J. Chem. Phys.* **1998**, *109*, 7005.
(3) Croce, F.; Persi, L.; Ronci, F.; Scrosati, B. *Solid State Ionics* **2000**, *135*, 47.
(4) Sandí, G.; Carrado, K. A.; Joachin, H.; Lu, W.; Prakash, J. *J. Power Sources* **2003**, *119*−*121*, 492.
(5) Fischer, H. *Mater. Sci. Eng. C* **2003**, *23*, 763.
(6) Takahashi, Y.; Sumita, I.; Tadokoro, H. *J. Polym. Sci.* **1973**, *11*, 2113.
(7) Takahashi, Y.; Tadokoro, H. *Macromolucules* **1973**, *6*, 672.
(8) Papke, B. L.; Ratner, M. A.; Shriver, D. F. *J. Phys. Chem. Solids* **1980**, *42*, 493.
(9) Marentette, J. M.; Brown, G. R. *Polymer* **1998**, *39*, 1405.
(10) Gu, F.; Bu, H.; Zhang, Z. *Macromol. Chem. Phys.* **1998**, *199*, 2597.
(11) Gu, F.; Bu, H.; Zhang, Z. *Polymer* **2000**, *41*, 7605.
(12) Ahlström, P.; Borodin, O.; Wahnström, G.; Wensink, E. J. W.; Carlsson, P.; Smith, G. D. *J. Chem. Phys.* **2000**, *112*, 10669.
(13) Borodin, O.; Douglas, R.; Smith, G. D.; Trouw, F.; Petrucci, S. *J. Phys. Chem.* **2003**, *107*, 6813.
(14) Blumberg, A. A.; Polack, S. S.; Hoeve, C. A. J. *J. Polym. Sci., Part A* **1964**, *2*, 2499.
(15) Ramana Rao, G.; Castiglioni, C.; Gussoni, M.; Zerbi, G. *Polymer* **1985**, *26*, 811.
(16) Chatani, Y.; Fujii, Y.; Takayanagi, T.; Honma, A. *Polymer* **1990**, *31*, 2238.
(17) Lihgtfoot, P.; Mehta, M. A.; Bruce, P. G. *J. Mater. Chem.* **1992**, *2*, 379.
(18) Bruce, P. G.; Campbell, S. A.; Lightfoot, P.; Mehta, M. A. *Solid State Ionics* **1995**, *78*, 191.
(19) Bruce, P. G. *Electrochim. Acta* **1995**, *40*, 2077.
(20) Palma, A.; Pasquarello, A.; Ciccotti, G.; Car, R. *J. Chem. Phys.* **1998**, *108*, 9933.
(21) Jeevanandam, P.; Vasudevan, S. *Chem. Mater.* **1998**, *10*, 1276.
(22) Johansson, P.; Tegenfeldt, J.; Lindgren, J. *Polymer* **2001**, *42*, 6573.
(23) Gadjiourova, Z.; Andreev, Y. G.; Tunstall, D. P.; Bruce, P. G. *Nature* **2001**, *412*, 520.
(24) Boulanger, P.; Magermans, C.; Verbist, J. J.; Delhalle, J.; Urch, D. S. *Macromolucules* **1991**, *24*, 2757.
(25) Boulanger, P.; Pireaux, J. J.; Verbist, J. J.; Delhalle, J. *Polymer* **1994**, *35*, 5185.
(26) Brena, B.; Luo, Y. *J. Chem. Phys.* **2003**, *119*, 7139.
(27) Pereira, R. P.; Rocco, A. M.; Bielschowsky, C. E. *J. Phys. Chem. B* **2004**, *108*, 12677.
(28) Frisch, M. J.; Trucks, G. W.; Schlegel, H. B.; Scuseria, G. E.; Robb, M. A.; Cheeseman, J. R.; Zakrzewski, V. G.; Montgomery, J. A., Jr.; Stratmann, R. E.; Burant, J. C.; Dapprich, S.; Millam, J. M.; Daniels, A. D.; Kudin, K. N.; Strain, M. C.; Farkas, O.; Tomasi, J.; Barone, V.; Cossi, M.; Cammi, R.; Mennucci, B.; Pomelli, C.; Adamo, C.; Clifford, S.; Ochterski, J.; Petersson, G. A.; Ayala, P. Y.; Cui, Q.; Morokuma, K.; Malick, D. K.; Rabuck, A. D.; Raghavachari, K.; Foresman, J. B.; Cioslowski, J.; Ortiz, J. V.; Stefanov, B. B.; Liu, G.; Liashenko, A.; Piskorz, P.; Komaromi, I.; Gomperts, R.; Martin, R. L.; Fox, D. J.; Keith, T.; Al-Laham, M. A.; Peng, C. Y.; Nanayakkara, A.; Gonzalez, C.; Challacombe, M.; Gill, P. M. W.; Johnson, B. G.; Chen, W.; Wong, M. W.; Andres, J. L.; Head-Gordon, M.; Replogle, E. S.; Pople, J. A. *Gaussian 98*, revision A.11; Gaussian, Inc.: Pittsburgh, PA, 2001.
(29) Gelius, U. *J. Electron Spectrosc. Relat. Phenom.* **1974**, *5*, 985.
(30) Yeh, J. J.; Lindau, I. *At. Data Nucl. Data Tables* **1985**, *32*, 1.
(31) Helgaker, T.; et al. *Dalton*, a molecular electronic structure program, Release 1.2 2001.

(32) Luo, Y.; Ågren, H.; Gel'mukhanov, F. *J. Phys. B* **1994**, *27*, 4169.
(33) Luo, Y.; Ågren, H.; Gel'mukhanov, F.; Guo, J.-H.; Skytt, P.; Wassdahl, N.; Nordgren, J. *Phys. Rev. B* **1995**, *52*, 14478.
(34) Brédas, J. L.; Salaneck, W. R. *J. Chem. Phys.* **1986**, *85*, 2219.
(35) Ortí, E.; Brédas, J. L. *J. Chem. Phys.* **1989**, *89*, 1009.
(36) DACAPO is free software developed at the Center for Atomic-Scale Material Physics (CAMP) funded by the Danish Research Council. www.fysik.dtu.dk/campos/Dacapo.
(37) Vanderbilt, D. *Phys. Rev. B* **1990**, *41*, 7892.
(38) Monkhorst, H. J.; Pack, J. D. *Phys. Rev. B* **1976**, *13*, 5188.
(39) Slusarczyk, Cz.; Suchocka-Galas, K.; Fabia, J.; Wlochowicz, A. *J. Appl. Crystallogr.* **2003**, *36*, 698.
(40) Wunderlich, B. *Macromolecular Physics*; Academic Press: New York, 1980.
(41) Warwick, T.; Heiman, P.; Mossessian, D.; McKinney, W.; Padmore, H. *Rev. Sci. Instrum.* **1995**, *66*, 2037.
(42) Nordgren, J.; Bray, G.; Cramm, S.; Nyholm, R.; Rubensson, J.-E.; Wassdahl, N. *Rev. Sci. Instrum.* **1989**, *60*, 1690.
(43) Lee, Y.; Choi, J.; Choi, Y.-W.; Sohn, D. *J. Phys. Chem. B* **2003**, *107*, 12373.